



HAL
open science

Solute Front Shear and Coalescence Control Concentration Gradient Dynamics in Porous Micromodel

Oshri Borgman, Régis Turuban, Baudouin Géraud, Tanguy Le Borgne, Yves
Méheust

► **To cite this version:**

Oshri Borgman, Régis Turuban, Baudouin Géraud, Tanguy Le Borgne, Yves Méheust. Solute Front Shear and Coalescence Control Concentration Gradient Dynamics in Porous Micromodel. *Geophysical Research Letters*, 2023, 50 (5), pp.e2022GL101407. 10.1029/2022gl101407. insu-04016281

HAL Id: insu-04016281

<https://insu.hal.science/insu-04016281>

Submitted on 6 Mar 2023

HAL is a multi-disciplinary open access archive for the deposit and dissemination of scientific research documents, whether they are published or not. The documents may come from teaching and research institutions in France or abroad, or from public or private research centers.

L'archive ouverte pluridisciplinaire **HAL**, est destinée au dépôt et à la diffusion de documents scientifiques de niveau recherche, publiés ou non, émanant des établissements d'enseignement et de recherche français ou étrangers, des laboratoires publics ou privés.

Geophysical Research Letters[®]

RESEARCH LETTER

10.1029/2022GL101407

Key Points:

- We analyze experimental pore-scale concentrations (c) and gradients over an extensive range of Pe
- The time of maximum c -gradient is predicted by the lamella mixing theory assuming simple shear flow
- The maximum c -gradient values are limited by aggregation between solute filaments

Supporting Information:

Supporting Information may be found in the online version of this article.

Correspondence to:

O. Borgman,
oshrib@migal.org.il

Citation:

Borgman, O., Turuban, R., Géraud, B., Le Borgne, T., & Méheust, Y. (2023). Solute front shear and coalescence control concentration gradient dynamics in porous micromodel. *Geophysical Research Letters*, 50, e2022GL101407. <https://doi.org/10.1029/2022GL101407>

Received 29 SEP 2022
Accepted 22 JAN 2023

Author Contributions:

Conceptualization: Oshri Borgman, Régis Turuban, Baudouin Géraud, Tanguy Le Borgne, Yves Méheust

Funding acquisition: Oshri Borgman, Tanguy Le Borgne, Yves Méheust

Investigation: Régis Turuban, Baudouin Géraud

Methodology: Oshri Borgman, Tanguy Le Borgne, Yves Méheust

Software: Oshri Borgman, Régis Turuban, Baudouin Géraud, Yves Méheust

Supervision: Tanguy Le Borgne, Yves Méheust


Visualization: Oshri Borgman

Writing – original draft: Oshri Borgman

© 2023. The Authors.

This is an open access article under the terms of the [Creative Commons Attribution-NonCommercial-NoDerivs License](https://creativecommons.org/licenses/by/4.0/), which permits use and distribution in any medium, provided the original work is properly cited, the use is non-commercial and no modifications or adaptations are made.

Solute Front Shear and Coalescence Control Concentration Gradient Dynamics in Porous Micromodel

Oshri Borgman^{1,2} , Régis Turuban^{1,3}, Baudouin Géraud¹, Tanguy Le Borgne¹ , and Yves Méheust¹ 

¹CNRS, Géosciences Rennes, UMR 6118, Univ Rennes, Rennes, France, ²Now at MIGAL – Galilee Research Institute, Kiryat Shmona, Israel, ³Scuola Internazionale Superiore di Studi Avanzati, Trieste, Italy

Abstract In subsurface environments, incomplete mixing at the pore scale limits reaction rates, rendering their prediction by Darcy-scale models challenging. Such pore scale concentration gradients are enhanced by the deformation of solute fronts and decay under the action of molecular diffusion and solute filament merging. It is currently unclear how these processes govern concentration gradient dynamics under different flow rates. We measure experimentally pore scale concentrations in solute fronts transported in a two-dimensional porous micromodel over an extensive range of flow rates. We demonstrate that pore-scale shear flow increases concentration gradients up to a time predicted by the lamellar mixing theory in shear flow. However, the flow rate-dependency of the mean concentration gradient at this so-called mixing time is weaker than predicted theoretically, a discrepancy which we explain quantitatively by accounting for lamellae aggregation. These findings shed new light on the pore-scale mechanisms driving mixing dynamics in porous media.

Plain Language Summary Solute mixing is the process that homogenizes chemical species' concentrations over space in time. Solute mixing rates are crucial to chemical reactions associated with environmental flow phenomena. Classical flow and transport models use solute concentration values averaged over length scales of a few millimeters and higher. But concentrations can show substantial variations at single pores' sub-millimetric length scales, which impact large-scale reaction rates. Besides, the heterogeneous porous structure of subsurface natural materials causes flow velocity variations between solid grains, which impact spatial variations of concentration within solute plumes. We present solute transport experiments in a flow cell mimicking the geometry of natural porous media. The transparent flow cell allows direct measuring of the concentration of a fluorescent dye injected at various flow rates to infer their impact on concentration variations. The recently introduced lamellar mixing theory describes the overall time dynamics of concentration variations well. However, the maximum mixing rates differ from theoretical predictions due to an additional mechanism currently not considered in the theory: the aggregation of solute lamellae. This work establishes the full relevance of the lamellar mixing theory to porous media flow when accounting for lamellae aggregation.

1. Introduction

Solute transport in porous media plays a central role in a variety of environmental processes. During their transport, solutes experience dispersion and mixing, two coupled but distinct processes (Ginn, 2018; Kitanidis, 1994). Dispersion controls the solute plume's spatial spreading, while mixing reduces the concentration variability within it (Dentz et al., 2011; Le Borgne et al., 2010). Solute mixing controls reaction rates in a range of processes when the typical reaction time is shorter than the typical mixing time (Chiogna et al., 2012; Engdahl et al., 2014; Rolle & Le Borgne, 2019; Valocchi et al., 2019), including groundwater contaminant transport and degradation (Kang et al., 2019), mineral dissolution and precipitation rates (Al-Khulaifi et al., 2019; Cil et al., 2017), mineral transformation at bacterial hot spots, bacterial growth rates and chemotaxis (Bochet et al., 2020; de Anna et al., 2021; Hubert et al., 2020), and CO₂ sequestration (Gilmore et al., 2020; MacMinn et al., 2012). An important feature of reactive transport by porous media flow is that often chemical species exhibit *incomplete mixing* at the pore scale, meaning that their concentrations are not uniform within individual pores (de Anna, Jiménez-Martínez et al., 2014; Gramling et al., 2002; Puyguiraud et al., 2020; Sole-Mari et al., 2022). This leads to discrepancies between reaction rates measured in laboratory batch systems and in porous media (Botella Espeso et al., 2021). The impact of incomplete mixing on precipitation and reaction rates was shown at the laboratory and the field scales (Cil et al., 2017; de Anna, Jiménez-Martínez et al., 2014; Kang et al., 2019).

Writing – review & editing: Régis Turuban, Baudouin Géraud, Tanguy Le Borgne, Yves Méheust

Concentration gradients play a key role in mixing dynamics and are a fundamental measure of solute mixing (Boon et al., 2017; de Dreuzy et al., 2012; De Simoni et al., 2005, 2007; Le Borgne et al., 2010). The dynamics and statistics of concentration gradients have been described and predicted by the lamella theory that quantifies the interplay between fluid deformation, which enhances gradients, and diffusion, which dissipates them (de Anna, Jiménez-Martínez et al., 2014; Jiménez-Martínez et al., 2017; Le Borgne et al., 2015, 2017; Souzy et al., 2018). The pore scale fluid deformation properties are governed by shear, driven by longitudinal velocity gradients (de Anna, Jiménez-Martínez et al., 2014; Dentz et al., 2016; Jiménez-Martínez & Negre, 2017) and chaotic deformation, induced by repeated stretching and folding patterns (Heyman et al., 2020; Souzy et al., 2020; Turuban et al., 2018). While the latter can only occur in 3D porous media under steady flows, shear deformation is ideally studied in 2D porous media. Under high Péclet (Pe) numbers, which quantify the characteristic diffusion to advection times ratio, the impact of deformation on concentration gradients is provided by simple analytical solutions (Villermaux, 2019). However, at intermediate Pe numbers relevant for porous media applications, elongated solute lamellae interact with each other and with grain walls (Hamada et al., 2020) due to confinement. The prediction of the temporal dynamics of concentration gradients as a function of Pe is, therefore, non-trivial.

In this study, we use millifluidic experiments to investigate the dynamics of concentration gradients and mixing in solute fronts traveling in a two-dimensional porous medium over a large range of Péclet numbers ($10^1 \leq Pe \leq 10^3$). We obtain highly resolved concentration and gradient fields and analyze their dynamics using the lamellar solute mixing theory. We quantify the evolution of lamellae number and their aggregation as the solute plume progresses in the porous medium. We thus demonstrate the impact of aggregation on solute gradients, which is responsible for the departure from the classical lamella theory prediction for simple shear flow. These findings provide new insights into the impact of flow on pore scale mixing dynamics in porous media.

2. Experiments

2.1. Setup

We perform conservative solute transport experiments in a two-dimensional analog porous medium. The flow cell is fabricated by optical lithography (see de Anna, Jiménez-Martínez et al., 2014); it consists of two parallel glass plates containing an array of polydisperse circular pillars mimicking solid grains. The pillars' positions were defined by a discrete element method (DEM) packing of discs with normally distributed diameters; the diameters were then scaled down to obtain a 2D porous medium. The flow cell inlet chamber is divided into two levels, allowing us to create a sharp solute front by circulating the solute between the two levels before injection into the porous medium (de Anna, Dentz, Tartakovsky, & Le Borgne, 2014). The field-of-view dimensions are width \times length = 142 \times 63 mm. The aperture between the parallel plates is 1 mm, and the porosity is 0.58. The field of view contains 577 pillars with an average diameter (\pm standard deviation) of $\bar{d} = 2.8$ mm (± 0.22 mm). The average pore diameter and throat width are $\lambda = 2.3$ mm (± 0.83 mm) and $a = 1.2$ mm (± 0.14 mm), respectively. The absolute permeability is 3.38×10^{-2} mm², calculated by 2D numerical simulations of depth-averaged Stokes flow (De et al., 2021), performed using the computational fluid dynamics software OpenFOAM® (See Text S2 in Supporting Information S1).

The liquid phase is a 60–40 (% weight) water–glycerol mixture. We use a 20 mg/L Fluorescein sodium salt (Sigma Aldrich, France) solution as the conservative fluorescent tracer. The mixture's viscosity and density are $\mu = 3.63 \times 10^{-3}$ Pa \cdot s and $\rho = 1.100 \times 10^3$ kg/m³, respectively (Takamura et al., 2012). The diffusion coefficient of fluorescein in the water–glycerol mixture is $D_m = 4.9 \times 10^{-10}$ m²/s (D'Errico et al., 2004). Flow and transport in this system are characterized respectively by the Reynolds and Péclet numbers, defined here as $Pe = \bar{v}a^2/(2D_m\lambda)$ and $Re = \rho\bar{v}a/\mu$, where \bar{v} is the average pore flow velocity. We perform 11 experiments and use a syringe pump to impose flow rates between 0.3 and 10.0×10^{-8} m³/s, yielding the following ranges for the Péclet and Reynolds numbers: $Pe \in [33; 1,104]$ and $Re \in [0.021; 0.698]$. In this Reynolds number range, we consider that Stokes flow conditions are fulfilled; that is, the flow regime and streamlines are independent of Re. The Reynolds number is thus irrelevant to solute mixing, which is entirely controlled by the Péclet number. Though the highest Re values approach 1, the resulting solute concentration fields do not indicate any non-linearities in the advecting flow. The experimental flow conditions are summarized in Table S1 in Supporting Information S1.

The flow cell is placed horizontally above a blue LED panel to illuminate and excite the tracer. It is initially filled with the background solution, containing a very low Fluorescein concentration. A continuous solute (Fluorescein)

pulse is then injected at a constant rate along the flow cell's upstream boundary. Images are taken at constant time intervals using a monochrome CCD camera (Princeton Instruments MegaPlus EC-11000, Teledyne Princeton Instruments, NJ, USA) with a spatial resolution of 0.037 mm per pixel. A sketch of our experimental setup is shown in Figure S1 in Supporting Information S1. The images' light intensity is converted to solute concentrations c based on a calibration curve. The magnitude of concentration gradients is then calculated numerically from the images. More details on the image processing are provided in Text S1 in Supporting Information S1. Note that our two-dimensional concentration field is an average of the three-dimensional concentration field over the porous medium's thickness (1 mm). Given the ratios of that thickness to the mean pore length (0.43) and mean pore throat (0.83), the velocity profile across the vertical gap is not parabolic but still varies significantly, and the concentration field is likely to also vary over the medium's thickness. This means that our experiment is not entirely equivalent to a fully two-dimensional system.

2.2. Rescaled Quantities of Interest

Denoting \bar{v} the average pore scale liquid velocity, we define the typical time needed by the fluid to travel one pore length as $t_{\text{ad}} = \lambda/\bar{v}$, and use it as the time scaling factor. The resulting non-dimensional time $\tau = t/t_{\text{ad}}$ then represents the number of pore lengths traveled by the fluid at a given time and indicates the mean solute front position in the porous medium. We consider the concentration field rescaled by the injected concentration, $C \equiv c/c_{\text{max}}$. We define its rescaled gradient as $\nabla C \equiv a \nabla c/c_{\text{max}}$ and denote ∇C the scalar norm (i.e., magnitude) of ∇C .

3. Theoretical Background

We briefly describe the basic concepts of the lamellar mixing theory (Le Borgne et al., 2015), used here as a reference model to quantify the enhancement and decay of concentration gradients under the action of fluid deformation and molecular diffusion.

3.1. The Lamellar Solute Mixing Theory—Mixing Time

We consider the continuous injection of a solute in a parallel flow through a two-dimensional (2D) porous medium, as in our experimental setup. The solute front, defined as the boundary of the continuous $C < 0.5$ region, is initially a straight line perpendicular to the mean flow direction (hereafter denoted the longitudinal direction). We assume that the concentration's variation in the direction perpendicular to the front is initially characterized by an error function-like dependence on the longitudinal coordinate (x). The corresponding profile of the initial concentration gradient's magnitude, ∇C , is thus Gaussian, of width s_0 . We define the concentration gradient field region where ∇C has significant values and whose transverse profile is the aforementioned Gaussian, as a *lamella*. As the solute front moves through a heterogeneous flow field, velocity variations stretch the front, thus increasing its length. Due to fluid incompressibility, this stretching of fluid elements leads to their compression along the direction perpendicular to the stretching, which compresses the solute front and decreases its width s . Conversely, molecular diffusion acts to weaken concentration gradients and increase s . Initially, stretching-induced compression of s dominates, resulting in an increase in ∇C , which is the driving force for diffusion. The increase in ∇C then enhances the diffusive broadening of s so that it eventually overcomes the solute front's advection-induced compression. This transition occurs at the *mixing time* (Le Borgne et al., 2015; Villermaux, 2019) at which the mixing width s is minimal and the concentration gradient $\nabla C \sim s^{-1}$ is at a maximum.

3.2. Mixing in Simple Shear Flow

As a reference model for predicting the concentration gradient dynamics, we first consider a simple shear flow, where the velocity component in the longitudinal direction v_x is the only non-zero component and varies linearly with the transverse spatial coordinate y . The shear rate $\dot{\gamma} = \partial v_x / \partial y$ is constant in time and space and proportional to the Péclet number. The mixing time and minimum mixing width for a solute lamella in such a simple shear flow are, respectively (Souzy et al., 2018; Villermaux, 2019)

$$t_{\text{mix}} \approx \dot{\gamma}^{-1} \left(3 \frac{\dot{\gamma} s_0^2}{D_m} \right)^{1/3} \sim \text{Pe}^{-2/3}, \quad (1)$$

$$\text{and } s(t_{\text{mix}}) = s_0 \sqrt{5(3\text{Pe})}^{-1/3}. \quad (2)$$

Increasing the Péclet number and the solute lamella's compression leads to a shorter mixing time and lamella width at the mixing time. The concentration gradient over the solute front can be estimated as $\nabla c = \Delta c/s$, with Δc and s , respectively, the solute concentration difference across the front and the solute front width. From the scaling of Equation 2, and assuming that Δc is independent of Pe at t_{mix} , one expects the following scaling law for the maximum concentration gradient:

$$\langle \nabla C \rangle(t_{\text{mix}}) = \frac{a \nabla c(t_{\text{mix}})}{c_{\text{max}}} \approx \frac{\Delta c(t_{\text{mix}})}{s} \sim \text{Pe}^{1/3}. \quad (3)$$

While the simple shear flow is a highly idealized representation of the complex spatial structure of porous media velocity fields, it was successful at predicting some properties of mixing in unsaturated flow conditions in a similar experimental system (Jiménez-Martínez et al., 2017). The mean fluid shear rate $\dot{\gamma} = \partial v_x / \partial y$ can be approximated by \bar{v}/λ , the ratio of the mean pore velocity to the average pore size. One important limitation of this model, however, is that it does not account for the phenomenon of aggregation, in which single thin lamellae eventually merge to form a broader lamella (de Anna, Jiménez-Martínez et al., 2014; Le Borgne et al., 2015). As we show below, lamellae aggregation plays an important role in concentration gradient dynamics.

4. Results and Discussion

4.1. Solute Concentration and Gradient Field Images

As expected, the structure of solute fronts depends on the Péclet number. At low Péclet number, the solute front is relatively compact, while at larger Pe , it is more stretched and distorted (Figure 1, Movies S1 and S3; Borgman et al., 2022). The solid pillars cause the solute front to fold, forming an array of high-gradient filaments. As mentioned in Section 3.1, we identify the elongated structures in the concentration gradient as *lamellae*. Dispersion also increases the mixing zone width, defined here as the region where C varies between 0.05 and 0.95. At low Péclet it is relatively narrow, while at high Péclet, a broad mixing region develops with several advanced solute filaments. We evaluate the *mixing rate* from the concentration gradient magnitude ∇C defined in Section 2.2. As the front is deformed by the porous structure, the concentration gradients tend to align perpendicular to the longitudinal direction (Figure 1, Movies S2 and S4; Borgman et al., 2022). Their magnitude generally increases with Pe . Several concentration gradient lamellae are found within a single pore (Figure 1b), indicating a strong variation of concentrations within it and the persistence of incomplete solute mixing at the pore scale, which is more evident at higher Pe (Sole-Mari et al., 2022).

4.2. Global Concentration Gradients and the Mixing Time

To quantitatively assess the Péclet number's impact on the mixing behavior, we first calculate the globally-averaged (i.e., over the entire flow field) concentration gradient $\langle \nabla C \rangle(t)$. For all Péclet numbers, the concentration gradients initially increase sharply until reaching a maximum value, and then decrease gradually with time. These dynamics can be understood from the lamellar mixing theory as detailed in Section 3.1. In this framework, the concentration gradient behaves inversely to the lamella width. The compression and then diffusive relaxation of the lamella width yields this enhancement and decay of concentration gradients. The time at which $\langle \nabla C \rangle$ reaches its maximum is the mixing time t_{mix} at which the mixing width is minimum (see Section 3.1). In Figure 2a, we show the time series of $\langle \nabla C \rangle$ for four selected experiments, and the time series for all 11 experiments are shown in Figure S2 in Supporting Information S1.

The simple shear flow model predicts that the mixing time scales as $t_{\text{mix}} \propto \text{Pe}^{-2/3}$ (Equation 1). In Figure 2b, we plot t_{mix} values as a function of Pe and find a power law behavior of exponent -0.71 ± 0.05 , consistent with the theory. This excellent match between our results and the theoretical prediction suggests that the simple shear flow assumption describes the mixing dynamics reasonably well, at least during the early stages of the solute mixing process. Another important result from the simple shear flow theory is the Pe -dependence of $\nabla C(t_{\text{mix}})$ (Equation 3). However, the maximum gradient is observed to only grow weakly with Pe , with a power law exponent of 0.07 ± 0.01 (Figure 2b). In Section 4.3 below, we propose a mechanism to explain the discrepancy between the theoretical and experimental values of $\langle \nabla C \rangle(t_{\text{mix}})$. Note that error bars on the data points in Figure 2b correspond

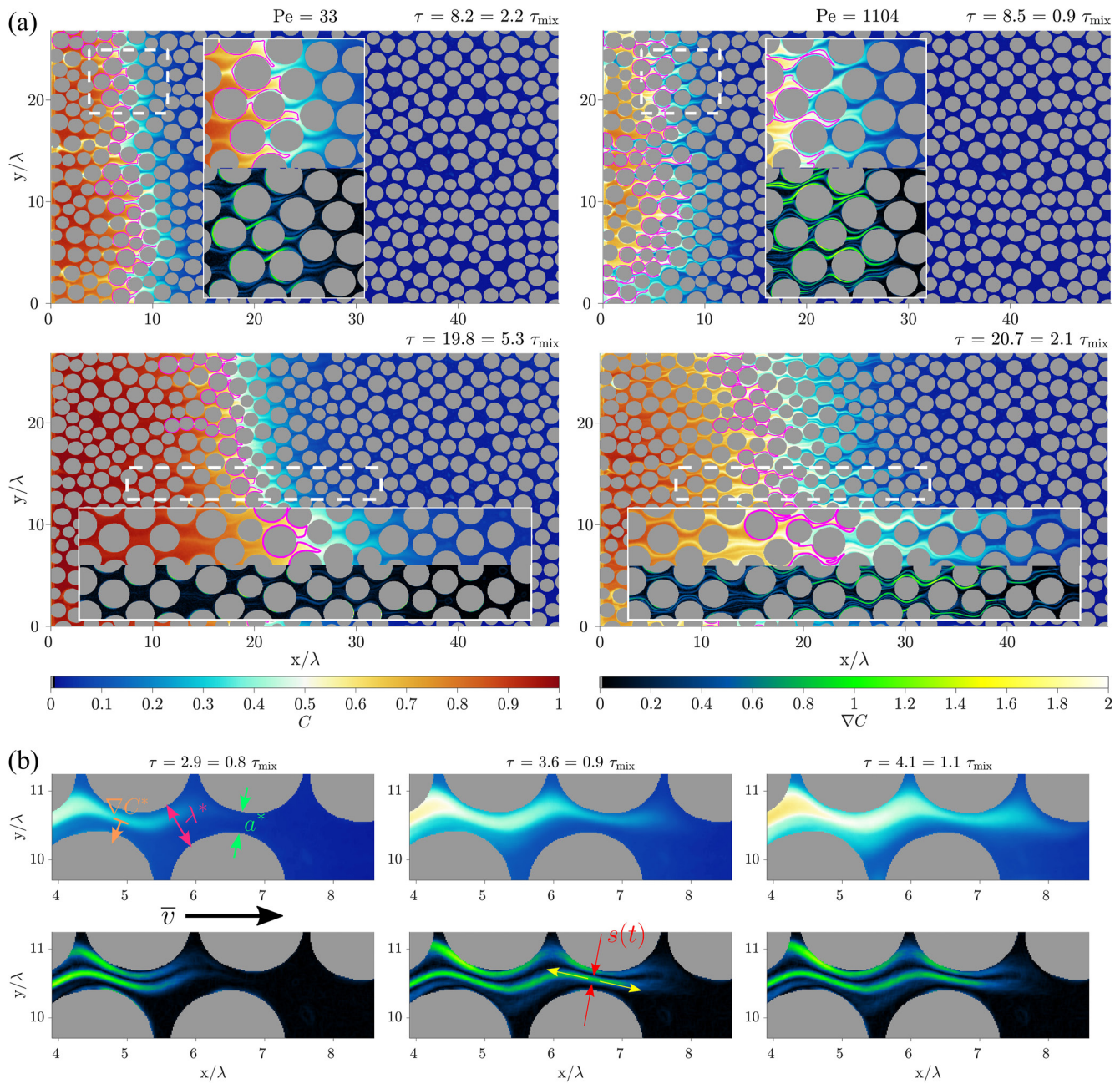


Figure 1. (a) Rescaled concentration fields C from two experiments with $Pe = 33$ (left) and $Pe = 1,104$ (right), at two non-dimensional times: $\tau \sim 8$ and 20 (top and bottom rows). The general flow direction is from left to right. Insets show C (upper) and its gradients' magnitude ∇C (lower) in the regions indicated by the dashed white frames in the large panels. The magenta line denotes the solute front in the main images and insets, and the gray discs denote solid pillars. The x range is shorter than the full flow cell length to improve image clarity. (b) Dynamics of one solute filament traveling with a mean velocity \bar{v} , showing the concentration and gradient fields (upper and lower rows, respectively) at three consecutive times. The local direction of the concentration gradient ∇C^* , the pore diameter λ^* , and the throat width a^* are indicated on the top left panel. As the lamella is stretched in the mean flow direction (middle-bottom panel, yellow arrows), it is compressed in the perpendicular direction (red arrows), and its width $s(t)$ decreases.

to the uncertainty on the measurements and that they are taken into account when estimating the uncertainty on the scaling law exponents. The uncertainty on the mixing time is due to the combined effect of the uncertainty on the estimated average gradient values and of their plateauing around the curve's maximum. More details are provided in Text S6 in Supporting Information S1.

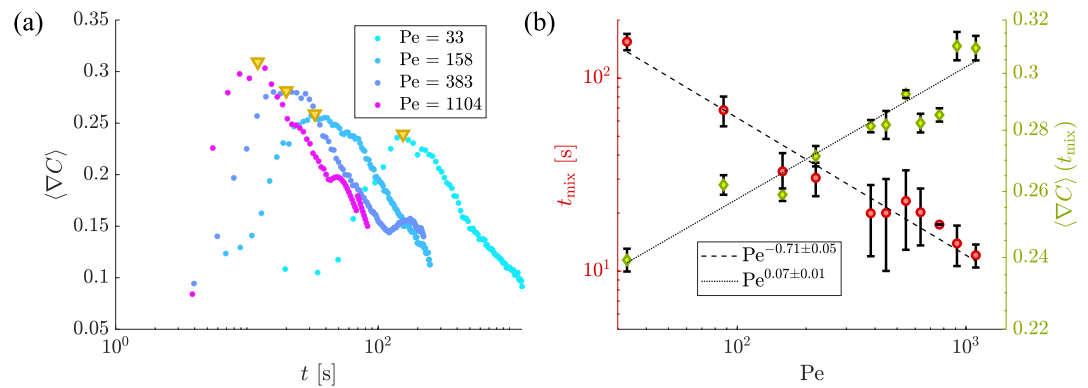


Figure 2. (a) The globally-averaged rescaled concentration gradient $\langle \nabla C \rangle$ versus time for four experiments with different Péclet numbers Pe . The mixing time t_{mix} , corresponding to the curves' maximum, is indicated by yellow inverted triangles in the plots. (b) t_{mix} is plotted as a function of Pe as red circles for all 11 experiments. The resulting power law behavior is consistent with the theoretical scaling $Pe^{-2/3}$, predicted by the simple shear flow model (Equation 1). The average concentration gradient at the mixing time $\langle \nabla C \rangle(t_{\text{mix}})$ is plotted as green diamonds, showing a weaker trend than the theoretically-predicted value of $Pe^{1/3}$. The error bars indicate the uncertainty in the mixing time and maximum gradient values, as explained in the text.

4.3. Effect of Lamellae Aggregation on Concentration Gradients

To understand the dynamics of concentration gradients, we infer the components of the gradients (Equation 3), namely the concentration differences Δc and the lamella width s . We calculate these components directly from c -field images by identifying the solute lamellae's structure (see Text S4 and S5 and Figures S3–S5 in Supporting Information S1). These estimations indicate that the average concentration difference at the mixing time, $\langle \Delta C \rangle(t_{\text{mix}})$, is independent of the Péclet, in consistency with the theoretical assumption made in the simple shear flow model. Furthermore, for the average solute lamella width $\langle \bar{s} \rangle(t_{\text{mix}})$ we obtain a scaling of $Pe^{-0.08}$ (Figure S5b in Supporting Information S1), showing a much weaker dependency on Pe than predicted by the simple shear model (Equation 2). This is consistent with the maximum concentration gradient's weak dependency on Pe (Figure 2b). The lamella width's dynamics are thus responsible for the departure from the simple shear flow model prediction.

We attribute this behavior to a lamellae aggregation mechanism induced by the flow geometry imposed by the porous medium structure. When the solute front flows through the porous medium, it folds upon hitting a solute grain. And as flow lines are condensed in pore throats downstream, two solute gradient filaments (i.e., lamellae) are brought closer together, which can result in their transverse aggregation (Figure 3c). This process increases the mean width of lamellae and thus reduces the concentration gradients. Such aggregation events are shown in the concentration gradient images in Figures 3a and 3b for two Pe values, just before and at the mixing time. We quantitatively assess the impact of lamellae aggregation on the average concentration gradient at t_{mix} by analyzing the lamellae number (N) dynamics. To calculate N , we consider the concentration field's cross-sections along the transverse direction and find their local minima and maxima. A lamella is a region between two consecutive local extrema (for more detail, see Text S4 and Figure S3 in Supporting Information S1).

The number of solute lamellae increases linearly with time during the early stages of the experiments, before t_{mix} (Figure 3d). This initial growth rate is controlled by the number of pillars that fold the front as it progresses in the porous medium. Therefore, the linear increase of N as a function of the mean longitudinal distance traveled by the front, τ , is independent of Pe (Figure 3e). After t_{mix} , when diffusion overcomes compression and increases the mean solute lamella width, the number of newly created lamellae is compensated by their aggregation, resulting in a constant N (Figures 3d and 3e). For low Péclet numbers, the transition between the initial linear increase is abrupt, while for high Pe , a more progressive transition between these two regimes is observed. The resulting number of lamellae in the solute front in this dynamic balance regime, $N(t > t_{\text{mix}})$, is plotted as a function of the Péclet number in Figure 3f; it has a weak but significant dependency on Pe , as Pe^α , with $\alpha = 0.111 \pm 0.002$. If aggregation strictly started at the mixing time, t_{mix} , we should have $N(t_{\text{mix}}) \sim vt_{\text{mix}} \sim Pe^{1/3}$. The exponent $\alpha < 1/3$, therefore, implies that aggregation starts to develop before the mixing time, and this all the more as the Péclet is larger. This likely results from the front's deeper penetration at the mixing time for high Péclet numbers, which favors lamellae aggregation events at pore throats.

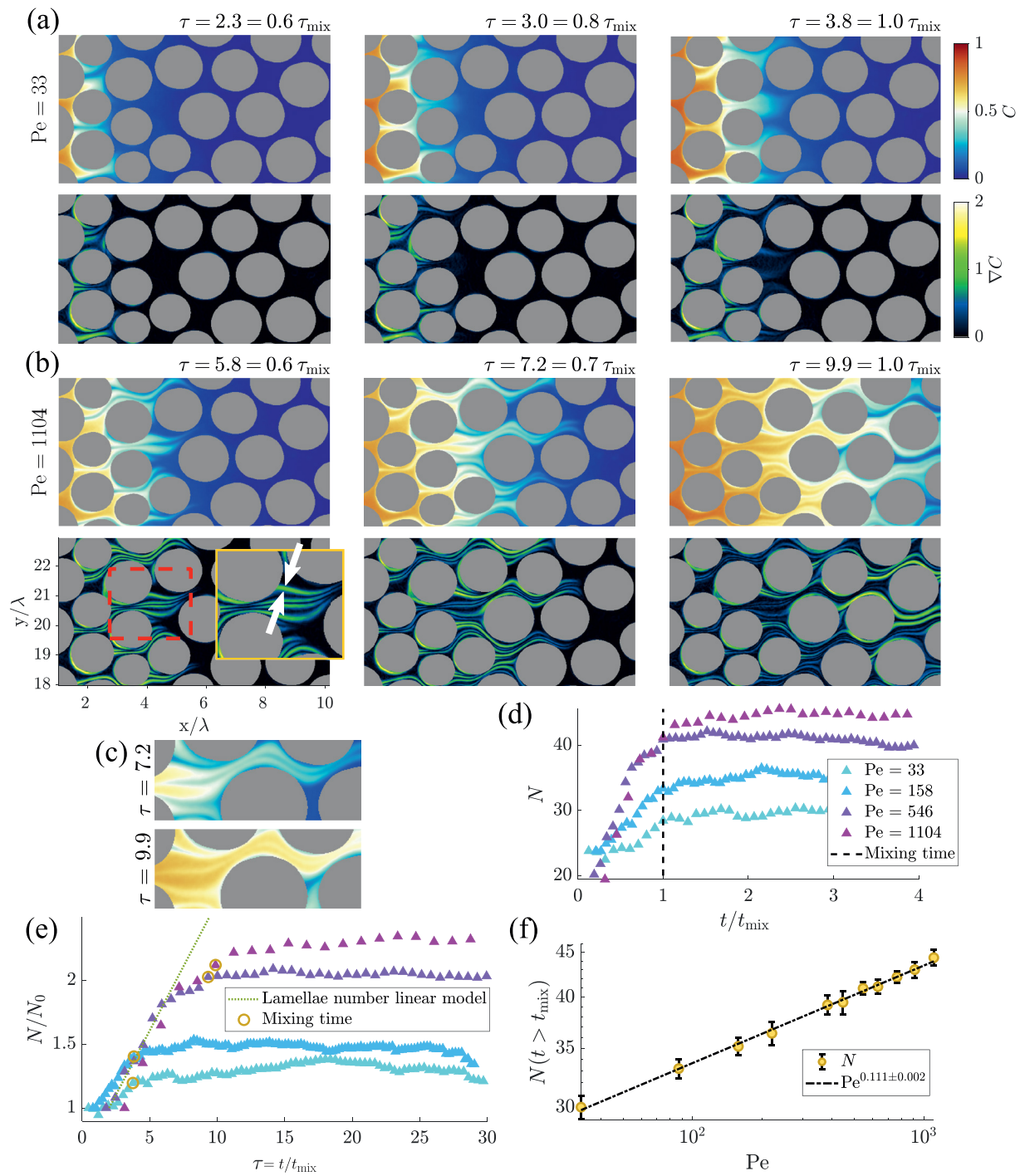


Figure 3. Solute concentrations C (upper row) and their gradients ∇C (lower row) in a small porous medium region (indicated by the axes on the bottom-left panel) for $Pe = 33$ (a) and 1,104 (b), at different rescaled times $\tau = t/t_{ad}$. The last panel for each Pe value corresponds to the mixing time. The inset for $Pe = 1,104$ at $\tau = 5.8$ shows the concentration gradients in the region denoted by the red dashed frame, with white arrows indicating a single lamella width. (c) The solute gradient filaments' (lamellae) aggregation process is shown by zooming in on a small section of the $Pe = 1,104$ C -field. (d) Average solute lamellae number N versus the time t rescaled by the mixing time t_{mix} . (e) Ratio of N to the initial lamellae number N_0 , as a function of the non-dimensional time $\tau = t/t_{ad}$. The green dashed line indicates the advection-controlled initial linear increase in lamellae number. Yellow circles indicate the mixing time. (f) The value of N at times larger than t_{mix} scales as Pe^α , with $\alpha = 0.111 \pm 0.002$. The error bars represent the standard deviation of N values within the plateaus in (d) and (e).

To quantify this effect, we define N_T , the total number of advective lamellae which would be created at infinite Péclet number (i.e., if no aggregation occurred). N_T is expected to increase linearly as

$$N_T \sim t/t_{ad}, \quad (4)$$

as explained above. We define s_{na} as the lamella width predicted by the shear flow theory in the absence of aggregation. Through aggregation, the joint width of all lamellae, $N_T s_{na}$, is redistributed into N effective lamellae, constructed from bundles of advective lamellae. The resulting average effective lamella width is

$$\langle s \rangle = s_{na} \frac{N_T}{N}. \quad (5)$$

From Equations 1 and 4, and the definition of t_{ad} , we have $N_T(t_{mix}) \propto Pe^{1/3}$. The number of effective lamellae at the mixing time, estimated from Figure 3f, follows $N(t_{mix}) = Pe^\alpha$. From Equation 2, we have $s_{na}(t_{mix}) \propto Pe^{-1/3}$, and thus the mean lamella width at the mixing time can be predicted to scale with the Péclet as

$$\langle s \rangle(t_{mix}) \propto \frac{Pe^{1/3} Pe^{-1/3}}{Pe^\alpha} \sim Pe^{-\alpha}. \quad (6)$$

From Equation 3, we finally obtain the scaling $\langle \nabla C \rangle \propto Pe^\alpha = Pe^{0.111}$. This exponent is close to the value directly measured from the concentration field (Figure 2), which is 0.07. These findings suggest that the discrepancy between the predictions from the simple shear-based lamella mixing model and our measurements is due to the transverse aggregation of lamellae constituting the solute front.

4.4. Impact of Porous Medium Structure

4.4.1. Impact of Heterogeneity in a 2D Porous Medium

It is likely that the exponent $\alpha = 0.111$ in the lamellae number at t_{mix} dependency on Péclet (Pe) (Figure 3f) is not universal. More generally, the scaling exponents for the dependence of the maximum gradient $\langle \nabla C \rangle(t_{mix})$ and mixing time t_{mix} on Pe , may depend on the porous medium's structure and heterogeneity. As long as advection by the fluid can be assimilated to a simple shear flow in the lamella theory of mixing, the scaling of t_{mix} with Pe should not change between different porous media. However, even in this case, we can expect that higher pore size disorder would impact the tendency for solute lamellae aggregation and thus impact the scaling of $\langle \nabla C \rangle(t_{mix})$ with Pe . For example, the ratio between throat width and pore (body) length will impact the results since (as shown in Figure 3c) lamellae aggregation appears to begin inside the pore body, where velocities are lower and stretching is locally reduced. Furthermore, it is likely that with more complex structures and a larger pore-scale heterogeneity, the mixing theory based on the simple shear flow model would not properly describe the scaling of t_{mix} with Pe , and the solid grains' shape and roughness may also play a role (Heyman et al., 2021). Although increased heterogeneity was already shown to increase fluid stretching rates in 2D Darcy-scale flow (Dentz et al., 2016), the effect of porous medium structure on pore-scale solute mixing still remains to be systematically investigated.

4.4.2. Impact of Dimensionality—3D Versus 2D Porous Media

In three-dimensional (3D) porous media, such as packings of grains or beads, both lamellae creation and aggregation could be amplified in comparison to 2D porous media. Stretching and folding of fluid elements in 3D porous media flow lead to exponential elongation of solute lamellae (Heyman et al., 2020; Souzy et al., 2020) rather than the algebraic elongation observed in a 2D system. As a result, in 3D porous media flow, the average concentration gradients (and thus, mixing rates) could potentially increase faster and to a much larger value than in 2D systems. However, since the exponential elongation of lamellae occurs in a finite domain, the aggregation rate is also expected to be larger in 3D porous media. Therefore, the balance between lamellae aggregation and stretching should be similar in 3D porous media as in this study. Most previous studies on 3D media have focused on very high Péclet numbers, where stretching dominates. Thus, the lamella aggregation phenomenon we report here has seldom been observed in 3D systems. Turuban et al. (2021) recently showed the aggregation of solute lamellae in a particulate suspension at low to intermediate Pe , indicating that solute lamellae aggregation would play a role in 3D flows as well. However, a quantitative investigation of this mechanism of concentration gradient limitation in 3D porous media remains to be addressed.

Note also that, as mentioned in Section 2.1, our system is not fully two-dimensional due to the influence of the top and bottom plates. However, the fluid stretching laws in the horizontal plane should not be affected, so we expect that the interpretation of 2D solute mixing in a full 2D system would be similar, with a possible change in the scaling exponent of the average concentration gradient's maximum value.

5. Conclusions

In this letter, we use solute transport experiments to investigate the dynamics of concentration gradients in a porous micromodel over an extensive range of Péclet numbers. High-resolution pore-scale imaging reveals the effect of flow rate on the concentration and gradient fields' spatial distribution and time evolution. Solute front stretching induces the compression of solute gradient lamellae, enhancing concentration gradients until the mixing time, after which the gradients start decaying under the action of diffusion. This so-called mixing time, at which concentration gradients are maximum, decreases as $Pe^{-0.71}$, a scaling that agrees well with the simple shear flow-based lamellar theory of mixing. The mean concentration gradient at the mixing time, $\langle \nabla C \rangle(t_{\text{mix}})$, however, shows a clear increase with Pe , but with a much weaker scaling exponent than predicted by the theory. We demonstrate that this weaker scaling of the concentration gradients with Pe results from lamellae aggregation.

As the solute front travels through the porous medium, new solute filaments appear by the front's advective folding around solid pillars, resulting in a linear increase of the number of lamellae in the concentration gradient, at a rate proportional to Pe , until lamellae start aggregating with each other. When the rate of lamellae destruction by aggregation balances their rate of creation by advective folding, the lamellae number reaches an asymptotically constant value at a time coinciding with the mixing time. For sufficiently high Pe values, lamellae aggregation begins before the mixing time, initiating a broad transition of the lamellae number from the linear advection-controlled regime to the dynamic balance plateau. Lamellae aggregation increases the mean lamella width and reduces the mean concentration gradient. It results in the maximum concentration gradient's aforementioned weaker scaling with Pe , as compared to the scaling predicted by the simple shear flow-based lamellar mixing model. From the measured scaling of the lamellae number in the dynamic balance plateau with the Péclet number, the lamellar mixing theory for simple shear flow can be complemented to account for lamellae aggregation and thus predict the maximum concentration gradient's correct scaling with Pe .

We thus show that while changing the Péclet impacts the time dependency of the mixing process, enhancing mixing by increasing Pe is by far not as efficient as predicted by the general lamellar mixing theory based on simple shear flow. Mixing enhancement appears to strongly depend on solute lamellae aggregation, which is controlled by the porous medium's structure. Therefore, future work should investigate the impact of varying porous medium heterogeneity on mixing enhancement, both in 2D and 3D porous media.

These findings provide new insights into the pore scale dynamics of mixing in porous media. In particular, concentration gradients play a key role in chemical reactions as well as microbiological processes. The new mechanisms uncovered here are key advances for the understanding and modeling of the timing and magnitude of concentration gradient enhancement by flow through porous media.

Data Availability Statement

The concentration field images and the data used for the figures in the study are available at Zenodo via <https://doi.org/10.5281/zenodo.7514283> with Creative Commons Attribution 4.0 International licence (Borgman et al., 2022).

References

- Al-Khulaifi, Y., Lin, Q., Blunt, M. J., & Bijeljic, B. (2019). Pore-scale dissolution by CO_2 saturated brine in a multimineral carbonate at reservoir conditions: Impact of physical and chemical heterogeneity. *Water Resources Research*, 55(4), 3171–3193. <https://doi.org/10.1029/2018WR024137>
- Bochet, O., Bethencourt, L., Dufresne, A., Farasin, J., Pédrot, M., Labasque, T., et al. (2020). Iron-oxidizer hotspots formed by intermittent oxic–anoxic fluid mixing in fractured rocks. *Nature Geoscience*, 13(2), 149–155. <https://doi.org/10.1038/s41561-019-0509-1>
- Boon, M., Bijeljic, B., & Krevor, S. (2017). Observations of the impact of rock heterogeneity on solute spreading and mixing. *Water Resources Research*, 53(6), 4624–4642. <https://doi.org/10.1002/2013WR015127>
- Borgman, O., Turuban, R., Géraud, B., Le Borgne, T., & Méheust, Y. (2022). Data for the manuscript titled "Solute front shear and coalescence control concentration gradient dynamics in porous micromodel" [Dataset]. Zenodo. <https://doi.org/10.5281/ZENODO.7514283>

Acknowledgments

Funding by the E.U. is gratefully acknowledged by O. Borgman, T. Le Borgne and Y. Méheust under the MSCA Individual Fellowship program (project *UnsatPorMix*, nr. 843594), and by B. Géraud, T. Le Borgne and Y. Méheust under the ERC program (Consolidator project *ReactiveFronts*, nr. 648377). O. Borgman and Y. Méheust are also grateful to the French National Agency for Research (ANR) for funding project *2PhlowFrac* (nr. ANR-20-CE92-0026).

- Botella Espeso, M., Corada-Fernández, C., García-Delgado, M., Candela, L., González-Mazo, E., Lara-Martín, P., & Jiménez-Martínez, J. (2021). Structural control of the non-ionic surfactant alcohol ethoxylates (AEOs) on transport in natural soils. *Environmental Pollution*, 269, 116021. <https://doi.org/10.1016/j.envpol.2020.116021>
- Chiogna, G., Hochstetler, D. L., Bellin, A., Kitanidis, P. K., & Rolle, M. (2012). Mixing, entropy and reactive solute transport. *Geophysical Research Letters*, 39(20), 20405. <https://doi.org/10.1029/2012GL053295>
- Cil, M. B., Xie, M., Packman, A. I., & Buscarnera, G. (2017). Solute mixing regulates heterogeneity of mineral precipitation in porous media. *Geophysical Research Letters*, 44(847), 6658–6666. <https://doi.org/10.1002/2017GL073999>
- De, N., Meunier, P., Méheust, Y., & Nadal, F. (2021). Bi-dimensional plume generated by the convective dissolution of an extended source of CO₂. *Physical Review Fluids*, 6(6), 063503. <https://doi.org/10.1103/PhysRevFluids.6.063503>
- de Anna, P., Dentz, M., Tartakovsky, A., & Le Borgne, T. (2014). The filamentary structure of mixing fronts and its control on reaction kinetics in porous media flows. *Geophysical Research Letters*, 41(13), 4586–4593. <https://doi.org/10.1002/2014GL060068>
- de Anna, P., Jiménez-Martínez, J., Tabuteau, H., Turuban, R., Le Borgne, T., Derrien, M., & Méheust, Y. (2014). Mixing and reaction kinetics in porous media: An experimental pore scale quantification. *Environmental Science & Technology*, 48(1), 508–516. <https://doi.org/10.1021/es403105b>
- de Anna, P., Pahlavan, A. A., Yawata, Y., Stocker, R., & Juanes, R. (2021). Chemotaxis under flow disorder shapes microbial dispersion in porous media. *Nature Physics*, 17(1), 68–73. <https://doi.org/10.1038/s41567-020-1002-x>
- de Dreuzy, J.-R., Carrera, J., Dentz, M., & Le Borgne, T. (2012). Time evolution of mixing in heterogeneous porous media. *Water Resources Research*, 48(6), 6511. <https://doi.org/10.1029/2011WR011360>
- Dentz, M., Le Borgne, T., Englert, A., & Bijeljic, B. (2011). Mixing, spreading and reaction in heterogeneous media: A brief review. *Journal of Contaminant Hydrology*, 120–121(C), 1–17. <https://doi.org/10.1016/j.jconhyd.2010.05.002>
- Dentz, M., Lester, D. R., Le Borgne, T., & de Barros, F. P. J. (2016). Coupled continuous-time random walks for fluid stretching in two-dimensional heterogeneous media. *Physical Review E*, 94(6), 061102. <https://doi.org/10.1103/PhysRevE.94.061102>
- D’Errico, G., Ortona, O., Capuano, F., & Vitagliano, V. (2004). Diffusion coefficients for the binary system glycerol + water at 25°C. A velocity correlation study. *Journal of Chemical & Engineering Data*, 49(6), 1665–1670. <https://doi.org/10.1021/jc049917u>
- De Simoni, M., Carrera, J., Sánchez-Vila, X., & Guadagnini, A. (2005). A procedure for the solution of multicomponent reactive transport problems. *Water Resources Research*, 41(11), 1–16. <https://doi.org/10.1029/2005WR004056>
- De Simoni, M., Sanchez-Vila, X., Carrera, J., & Saaltink, M. W. (2007). A mixing ratios-based formulation for multicomponent reactive transport. *Water Resources Research*, 43(7), 1–10. <https://doi.org/10.1029/2006WR005256>
- Engdahl, N. B., Benson, D. A., & Bolster, D. (2014). Predicting the enhancement of mixing-driven reactions in nonuniform flows using measures of flow topology. *Physical Review E*, 90(5), 51001. <https://doi.org/10.1103/PhysRevE.90.051001>
- Gilmore, K. A., Neufeld, J. A., & Bickle, M. J. (2020). CO₂ dissolution trapping rates in heterogeneous porous media. *Geophysical Research Letters*, 47(12), e2020GL087001. <https://doi.org/10.1029/2020GL087001>
- Ginn, T. R. (2018). Modeling bimolecular reactive transport with mixing-limitation: Theory and application to column experiments. *Water Resources Research*, 54(1), 256–270. <https://doi.org/10.1002/2017WR022120>
- Gramling, C. M., Harvey, C. F., & Meigs, L. C. (2002). Reactive transport in porous media: A comparison of model prediction with laboratory visualization. *Environmental Science & Technology*, 36(11), 2508–2514. <https://doi.org/10.1021/es0157144>
- Hamada, M., Cueto-Felgueroso, L., & de Anna, P. (2020). Diffusion limited mixing in confined media. *Physical Review Fluids*, 5(12), 124502. <https://doi.org/10.1103/PhysRevFluids.5.124502>
- Heyman, J., Lester, D. R., & Borgne, T. L. (2021). Scalar signatures of chaotic mixing in porous media. *Physical Review Letters*, 126(3), 34505. <https://doi.org/10.1103/PhysRevLett.126.034505>
- Heyman, J., Lester, D. R., Turuban, R., Méheust, Y., & Le Borgne, T. (2020). Stretching and folding sustain microscale chemical gradients in porous media. *Proceedings of the National Academy of Sciences of the United States of America*, 117(24), 13359–13365. <https://doi.org/10.1073/pnas.2002858117>
- Hubert, A., Aquino, T., Tabuteau, H., Méheust, Y., & Le Borgne, T. (2020). Enhanced and non-monotonic effective kinetics of solute pulses under Michaelis–Menten reactions. *Advances in Water Resources*, 146, 103739. <https://doi.org/10.1016/j.advwatres.2020.103739>
- Jiménez-Martínez, J., Le Borgne, T., Tabuteau, H., & Méheust, Y. (2017). Impact of saturation on dispersion and mixing in porous media: Photobleaching pulse injection experiments and shear-enhanced mixing model. *Water Resources Research*, 53(2), 1457–1472. <https://doi.org/10.1002/2016WR019849>
- Jiménez-Martínez, J., & Negre, C. F. A. (2017). Eigenvector centrality for geometric and topological characterization of porous media. *Physical Review E*, 96(1), 013310. <https://doi.org/10.1103/PhysRevE.96.013310>
- Kang, P. K., Bresciani, E., An, S., & Lee, S. (2019). Potential impact of pore-scale incomplete mixing on biodegradation in aquifers: From batch experiment to field-scale modeling. *Advances in Water Resources*, 123, 1–11. <https://doi.org/10.1016/j.advwatres.2018.10.026>
- Kitanidis, P. K. (1994). The concept of the dilution index. *Water Resources Research*, 30(7), 2011–2026. <https://doi.org/10.1029/94WR00762>
- Le Borgne, T., Dentz, M., Bolster, D., Carrera, J., de Dreuzy, J.-R. R., & Davy, P. (2010). Non-Fickian mixing: Temporal evolution of the scalar dissipation rate in heterogeneous porous media. *Advances in Water Resources*, 33(12), 1468–1475. <https://doi.org/10.1016/j.advwatres.2010.08.006>
- Le Borgne, T., Dentz, M., & Villermaux, E. (2015). The lamellar description of mixing in porous media. *Journal of Fluid Mechanics*, 770, 458–498. <https://doi.org/10.1017/jfm.2015.117>
- Le Borgne, T., Huck, P. D., Dentz, M., & Villermaux, E. (2017). Scalar gradients in stirred mixtures and the deconstruction of random fields. *Journal of Fluid Mechanics*, 812, 578–610. <https://doi.org/10.1017/jfm.2016.799>
- MacMinn, C. W., Neufeld, J. A., Hesse, M. A., & Huppert, H. E. (2012). Spreading and convective dissolution of carbon dioxide in vertically confined, horizontal aquifers. *Water Resources Research*, 48(11), 1–11. <https://doi.org/10.1029/2012WR012286>
- Puyguraud, A., Perez, L. J., Hidalgo, J. J., & Dentz, M. (2020). Effective dispersion coefficients for the upscaling of pore-scale mixing and reaction. *Advances in Water Resources*, 146, 103782. <https://doi.org/10.1016/j.advwatres.2020.103782>
- Rolle, M., & Le Borgne, T. (2019). Mixing and reactive fronts in the subsurface. *Reviews in Mineralogy and Geochemistry*, 85(1), 111–142. <https://doi.org/10.2138/rmg.2018.85.5>
- Sole-Mari, G., Bolster, D., & Fernández-García, D. (2022). A closer look: High-resolution pore-scale simulations of solute transport and mixing through porous media columns. *Transport in Porous Media*, 146(1–2), 1–27. <https://doi.org/10.1007/S11242-021-01721-Z>
- Souzy, M., Lhuissier, H., Méheust, Y., Le Borgne, T., & Metzger, B. (2020). Velocity distributions, dispersion and stretching in three-dimensional porous media. *Journal of Fluid Mechanics*, 891, A16. <https://doi.org/10.1017/jfm.2020.113>
- Souzy, M., Zaier, I., Lhuissier, H., Le Borgne, T., & Metzger, B. (2018). Mixing lamellae in a shear flow. *Journal of Fluid Mechanics*, 838, R3. <https://doi.org/10.1017/jfm.2017.916>

- Takamura, K., Fischer, H., & Morrow, N. R. (2012). Physical properties of aqueous glycerol solutions. *Journal of Petroleum Science and Engineering*, 98–99, 50–60. <https://doi.org/10.1016/j.petrol.2012.09.003>
- Turuban, R., Lester, D., Le Borgne, T., & Méheust, Y. (2018). Space-group symmetries generate chaotic fluid advection in crystalline granular media. *Physical Review Letters*, 120(2), 024501. <https://doi.org/10.1103/PhysRevLett.120.024501>
- Turuban, R., Lhuissier, H., & Metzger, B. (2021). Mixing in a sheared particulate suspension. *Journal of Fluid Mechanics*, 916, 1–12. <https://doi.org/10.1017/jfm.2021.270>
- Valocchi, A. J., Bolster, D., & Werth, C. J. (2019). Mixing-limited reactions in porous media. *Transport in Porous Media*, 130(1), 157–182. <https://doi.org/10.1007/s11242-018-1204-1>
- Villermaux, E. (2019). Mixing versus stirring. *Annual Review of Fluid Mechanics*, 51(1), 245–273. <https://doi.org/10.1146/annurev-fluid-010518-040306>